Petroleum Science 20 (2023) 3723–3735

Contents lists available at ScienceDirect

Petroleum Science

journal homepage: www.keaipublishing.com/en/journals/petroleum-science

Original Paper

Visualization of hydraulic fracture interacting with pre-existing fracture

Zi-Xiao Xie, Xiao-Guang Wu, Teng-Da Long, Zhong-Wei Huang*, Gen-Sheng Li, Wen-Chao Zou, Zhao-Wei Sun

State Key Laboratory of Petroleum Resources and Prospecting, China University of Petroleum-Beijing, Beijing, 102249, China

ARTICLE INFO

Article history:
Received 20 June 2022
Received in revised form
8 May 2023
Accepted 19 July 2023
Available online 20 July 2023

Edited by Jia-Jia Fei

Keywords:
Hydraulic fracturing
Natural fracture
Fracture propagation
Interaction mode
PMMA

ABSTRACT

Hydraulic fracturing is considered the main stimulation method to develop shale gas reservoirs. Due to its strong heterogeneity, the shale gas formation is typically embedded with geological discontinuities such as bedding planes and natural fractures. Many researchers realized that the interaction between natural fractures and hydraulic fractures plays a crucial role in generating a complex fracture network. In this paper, true tri-axial hydraulic fracturing tests were performed on polymethyl methacrylate (PMMA), on which pre-existing fracture was pre-manufactured to simulate natural fracture. A cohesive model has been developed to verify the results of the experimental tests. The key findings demonstrate that the experimental results agreed well with the numerical simulation outcomes where three main interaction modes were observed: crossing; being arrested by opening the pre-existing fracture; being arrested without dilating the pre-existing fracture. Crossing behavior is more likely to occur with the approaching angle, horizontal stress difference, and injection rate increase. Furthermore, the higher flow rate might assist in reactivating the natural fractures where both sides of the pre-existing fractures were reactivated as the injection rate increased from 5 to 20 mL/min. Additionally, hydraulic fractures show a tendency to extend vertically rather than along the direction of maximum horizontal stress when they are first terminated at the interface. This research may contribute to the field application of hydraulic fracturing in shale gas formation.

1. Introduction

Shale gas, one of the major unconventional resources, is particularly heterogeneous with low porosity and permeability. There is a need to stimulate the shale gas reservoir in order to enhance its recovery and develop economically (Zeng et al., 2015; Zhang et al., 2015; Zhao et al., 2021). The hydraulic fracturing technique has been utilized for decades which can create complex fracture networks at the target zone by high-pressure water injected (Cong et al., 2022). Shale gas formation was typically embedded with geological discontinuities such as bedding planes, joints, and natural fractures which are the vital storage place for the oil and gas (Gale et al., 2014; Zhao et al., 2020b). However, many field applications demonstrated that natural fractures have a significant influence on the propagation of hydraulic fractures (Gale et al., 2007; Zou et al., 2016a; Li et al., 2020; Fu et al., 2021; Zhang et al., 2021; Memon et al., 2022). According to the coring samples of several typical shale reservoirs, it is found that there are a large number of cemented natural fractures filled with minerals such as quartz and calcite acting as weak planes (Zhao et al., 2020a). Microseismic monitoring results have indicated that hydraulic fractures could activate natural fractures forming complex fracture networks under certain conditions. Other works from DTS/DAS implied that partial penetration or even impeded fracture growth would occur due to the thin natural fractures or laminations in the reservoir (Xie et al., 2020). It is commonly agreed that the interaction between hydraulic fractures and pre-existing discontinuity is the key to enhancing the permeability of shale gas reservoirs (Hou et al., 2016; Zhou et al., 2016). However, there is still a lack of understanding of the propagation of hydraulic fractures when it interacts with pre-existing fractures due to limited monitoring methods (Roshankhah et al., 2018, 2019; Xie et al., 2021).

Several researchers have studied the influence of pre-existing

* Corresponding author.
E-mail address: huangzw@cup.edu.cn (Z.-W. Huang).

https://doi.org/10.1016/j.petsci.2023.07.014

fractures on hydraulic fracture propagation based on laboratory tests (Zhou et al., 2007; Gu et al., 2012; Kolawole and Ispas, 2020). It is widely believed that horizontal stress difference and approaching angle are the two main factors affecting whether the hydraulic fracture could cross the natural fractures or not (Zhang et al., 2020a; Kolawole and Ispas, 2020). Many test results showed that hydraulic fractures tend to be arrested by pre-existing fractures at low horizontal stress differences and small approaching angles (Zhou et al., 2010; Fatahi et al., 2017). Notably, the growth of fracture is also restricted by properties of the natural fractures, including interface shear strength, tensile strength, frictional strength, etc. Previous experiments showed that mineral composition inside the natural fractures affects the frictional properties of fracturing which hugely impacts the interaction behaviors between the natural fractures and hydraulic fractures. Artificial specimens with different strength cemented natural fractures also had been investigated, the results indicated that the hydraulic fractures would be arrested by weakly bonded natural fractures (Fu et al., 2015). Whereas, the hydraulic fracture was more prone to cross the natural fractures with strongly bonded natural fractures, concluding that the mechanical property of weak planes significantly influenced the propagation of hydraulic fracture (Wang et al., 2018; Liu et al., 2022a, b). Moreover, some researchers found that the width of the natural fracture also plays a vital role in affecting the fracture interaction mode. It is observed that the larger size of the natural fracture, the less chance for hydraulic fractures to cross the natural fractures (Dong et al., 2018; Xie et al., 2022).

However, it is virtually impossible to observe the interactions between hydraulic fractures and pre-existing fractures while fracturing the rock samples. Indirect methods, such as acoustic emissions (AE), have been used to infer the geometry of hydraulic fractures, but they could not clearly indicate the interactions behaviors between the hydraulic fractures and the pre-existing fractures (Groenenboom et al., 1995; Frash, 2014). Moreover, the spatial resolution of the AE signal is relativity low compared to the size of fractures (Roshankhah et al., 2018). CT scanning is another way to obtain the geometry of the fracture networks (Guo et al., 2014; Zou et al., 2016b). Despite CT scanning showing a better spatial resolution of the fracture geometry than AE monitoring, it still has some disadvantages. For instance, it is not able to present the process of hydraulic fracture propagation and only capable of scanning rock specimens less than 100 mm^3 (Liu et al., 2019; Li and Zang, 2021).

Polymethyl methacrylate (PMMA) is a transparent thermoplastic often used as a substitute for natural rocks because of its optical transparency, allowing visual assessment of the process of hydraulic fracturing without using sophisticated techniques such as AE and CT (Roshankhah et al., 2018; Li and Zhou, 2022). Another advantage of using PMMA as the specimen is its proximity to the mechanical properties of the shale gas formation. Although the tensile strength of the PMMA is rather high, the fracture toughness which is the dominant factor that influenced the cracking behaviors exhibits relatively similar values between the PMMA and shale. Additionally, the PMMA material presents a strong brittleness behavior showing a similar failure pattern with shale. Therefore, several researchers have conducted hydraulic fracturing experimental tests of PMMA to study fracture propagation behaviors (Wu et al., 2008; Zhou et al., 2018; Dong et al., 2021). The effect of confining stress, temperature, and borehole diameter on hydraulic fracturing was investigated using PMMA samples. In addition, water-less fracturing such as liquid nitrogen fracturing and supercritical CO_2 fracturing was tested on PMMA samples, allowing to observe of the pattern of the fracture network without opening up the specimens (Zhou et al., 2018; Hong et al., 2020).

So far, the previous research was primarily focused on whether the hydraulic fracture could be arrested by the natural fracture or not (Kolawole and Ispas, 2020). To our knowledge, few experiments have been conducted to visually present the process of hydraulic fractures interacting with pre-existing fractures. Therefore, in this paper, we conducted true triaxial hydraulic fracturing tests on PMMA specimens with pre-existing fractures. The propagation of hydraulic fractures was analyzed and the interactions behaviors between hydraulic fractures and pre-existing fractures were investigated. Main factors including in-situ stress difference, approaching angle, and injection rate were quantitatively investigated to figure out their effect on fracture interaction behaviors. Moreover, the propagation process of hydraulic fracture encounters with pre-existing fractures was captured by a high-speed video camera. A hydro-mechanical model was developed by the cohesive zone method and the experimental results agreed well with the numerical simulations. The key findings give us a better understanding of fracture interaction behaviors and provide theoretical guidance for the hydraulic fracturing of shale gas reservoirs.

The remainder of this paper is organized as follows. Section 2 describes the experimental procedure and sample preparation. Section 3 elucidates the results of the experimental tests. Section 4 presents the numerical simulation cases developed by the cohesive zone model. Section 5 gives a discussion about fracture interaction modes and the reasons why the experimental results show some degree of discrepancy with the theory. Lastly, the summaries and conclusions were presented in Section 6.

2. Experimental set-up and sample preparation

2.1. Experimental set-up

The tests were performed on a self-developed true triaxial pressure loading system. The experimental setup is shown in Fig. 1 which mainly consists of a water injection system, a true triaxial loading system, and a computer control system. The water injection system is capable of pressurizing water (up to 60 MPa) in the borehole by a servo-hydraulic pump with a constant flow rate of up to 50 mL/min. The true triaxial loading system was developed to simulate in-situ stress by exerting pressure in three directions. It mainly consists of two parts: a cubic loading chamber and hand piston pumps used for manually adjusting the pressure loaded on the confining plates. The cubic chamber can place specimens within the size of 200 mm cubes. The maximum confining stress is able to reach up to 20 MPa depending on the size of the specimen. The top platen of the chamber was centrally opened with a 20 mm diameter hole to make sure the water injection line is able to connect with the borehole. The computer control system is composed of data acquisition software and pressure sensors. The

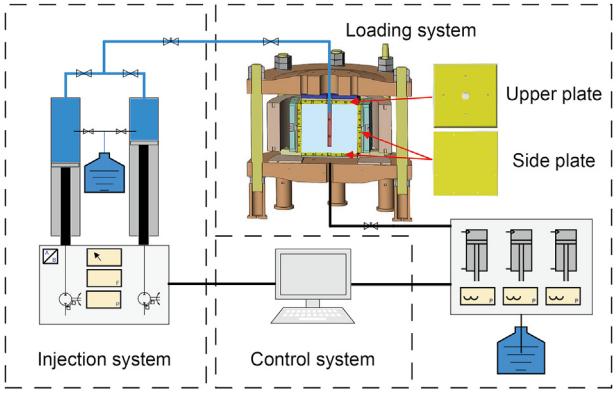

Fig. 1. Schematic of the true tri-axial hydraulic fracturing experimental set-up.

computer control system can control and monitor the water injection system, and the pressure data and the pumping rate will be automatically recorded into the computer during the fracturing process.

The experimental procedure is as follows:

(1) Install the testing specimen in the loading chamber and check the pipelines are connected correctly.
(2) Open the valves between the chamber and the hand piston pump, then load the specimen gradually until it reaches the target pressure.
(3) Open the valve mounted on the injection pipeline. Set a certain value of water injection rate on the computer control system and start the syringe pump. During the test, the loading value, injection pressure, and pumping rate are automatically recorded.
(4) After successfully fracturing the specimen, stop injecting water, save the data, and release the confining pressure loaded on the specimen. Take the specimen out of the chamber and close all valves.
(5) Repeat the procedure above to finish all the tests.

2.2. Sample preparation

To visually observe the initiation and propagation of hydraulic fracture, we conducted hydraulic fracturing tests on PMMA cubes with the size of 100 mm^3. A simulated borehole with a diameter of 16 mm is drilled to 60 mm in depth at the center of the surface. An inner diameter of 12 mm stainless steel tube was cemented with epoxy into the model borehole leaving a 20 mm open hole at the bottom for fracturing. Additionally, the upper 40 mm of the borehole was processed with screw threads to increase the contact area between epoxy and borehole, improving the sealing quality of the wellbore. As mentioned before, the tensile strength of the PMMA is relatively high, and there is almost no leak-off during the fracturing process, resulting in the breakdown pressure being relatively high (up to 35 MPa). The lower the breakdown pressure, the lower risk of seal leakage. Thus, two 10 mm high, 2 mm deep V-shape notches were induced symmetrically at the bottom of the borehole to decrease the breakdown pressure promoting the initiation of the hydraulic fractures, as shown in Fig. 2(a). Additionally, the preset notches are all along the direction of maximum principle stress, by doing so, the direction of hydraulic fractures initiation would be notch-originated propagating along with the direction of the maximum principle stress, and then the approaching angle would be close to what we have assumed. The mechanical properties of the sample are summarized in Table 1.

One of the main reasons for using PMMA as test samples is the flexibility of producing natural fractures inside the rock. In contrast, the properties of natural fractures in the natural rock present strong anisotropy which make it difficult to compare one to another. We first simulated three different kinds of analogue natural fractures by altering the glued area between the bonded interfaces (fully glued interface, partially glued interface, grooved glued interface) in the pre-tests (the test results were not presented in this work). The pre-tests result stated that PMMA samples with the fully glued interface produced highly repeatable outcomes where crossing and arresting behaviors were able to occur (Xie et al., 2021). Whereas, the predefined glued areas were not well controlled for partially glued interfaces and grooved glued interfaces, the final fracture geometries exhibited multiple outcomes under the same conditions. Natural fractures simulated in this way result in too much uncertainty when studying the influences of different factors on hydraulic fractures, as samples vary greatly from each case. Therefore, we simulated the natural fractures with desired and repeatable geometry by fully gluing PMMA plates together for the rest of the tests.

Thus, we applied the same method in this experimental test to pre-fracture the specimen. Three PMMA plates with certain thicknesses were stacked together at different angles according to the direction of initiation of hydraulic fracture. Three different angles (30°, 60°, 90°) were set to investigate the influence of the approaching angle on fracture propagation. The interfaces between PMMA plates were glued with fast-drying high-strength PMMA glue acting as the pre-existing fractures inside the specimen. Fig. 2(b–d) showed a sketch of the pre-fractured PMMA with different bounding angles. We defined approaching angles (α) as the angle between the direction of the pre-fractured interface and the direction of maximum horizontal stress.

2.3. Experimental scheme and procedure

Nine groups of tests were conducted to investigate the effect of horizontal stress difference, approaching angle, and injection rate on fracture interaction behavior, respectively. The direction of minimum horizontal stress is perpendicular to the direction of the initial crack in order to facilitate the hydraulic fracture initiated from the notch. As mentioned above, an initial set of pre-tests were conducted on the PMMA sample to investigate the feasibility of the experiments and the results indicated that our method for testing is reliable and repeatable, which were not shown in the table below. The horizontal stress difference coefficient is defined in Eq. (1)

$$K_h = \frac{\sigma_H - \sigma_h}{\sigma_h} \tag{1}$$

In which K_h is the horizontal stress difference coefficient, σ_H [MPa] is the maximum horizontal in-situ stress, and σ_h [MPa] is the minimum horizontal in-situ stress. The magnitude of the applied confining stress and injection rate was chosen based on our previous experimental tests. A summary of the test parameters is shown in Table 2.

3. Experimental results analysis

3.1. Fracture morphology of hydraulic fracture interacting with pre-existing fracture

After fracturing the specimens, we observed PMMA specimens under green laser irradiation to clearly identify the fracture geometry and took photos from the bottom side of the view. Fig. 3 shows the fracture morphology of PMMA specimens at different approaching angles. It clearly showed that three types of fracture interaction behaviors were observed: i. Hydraulic fracture crossed pre-existing fractures (#1); ii. Pre-existing fractures impeded hydraulic fracture without being reactivated (#2); iii. The arrest of hydraulic fracture by reactivating the pre-existing fractures (#3). As shown in Fig. 3, the hydraulic fracture was initiated from the initial notch perpendicular to the direction of minimum horizontal stress (σ_h), and then propagated along the maximum horizontal stress (σ_H) until encountered the pre-existing fracture. In the case of #1 (Fig. 3(a)), a bi-wing fracture was formed penetrating both sides of pre-existing fracture with the approaching angle of $\theta = 90°$. After intersecting with the interface, hydraulic fractures continued to extend along the direction of maximum horizontal stress until they reached the exterior of the specimen and did not activate any of the pre-existing fractures. When the approaching angle between hydraulic fracture and natural fracture decreased to $\theta = 60°$ (Fig. 3(b)), only one side of pre-existing fracture was crossed and another wing

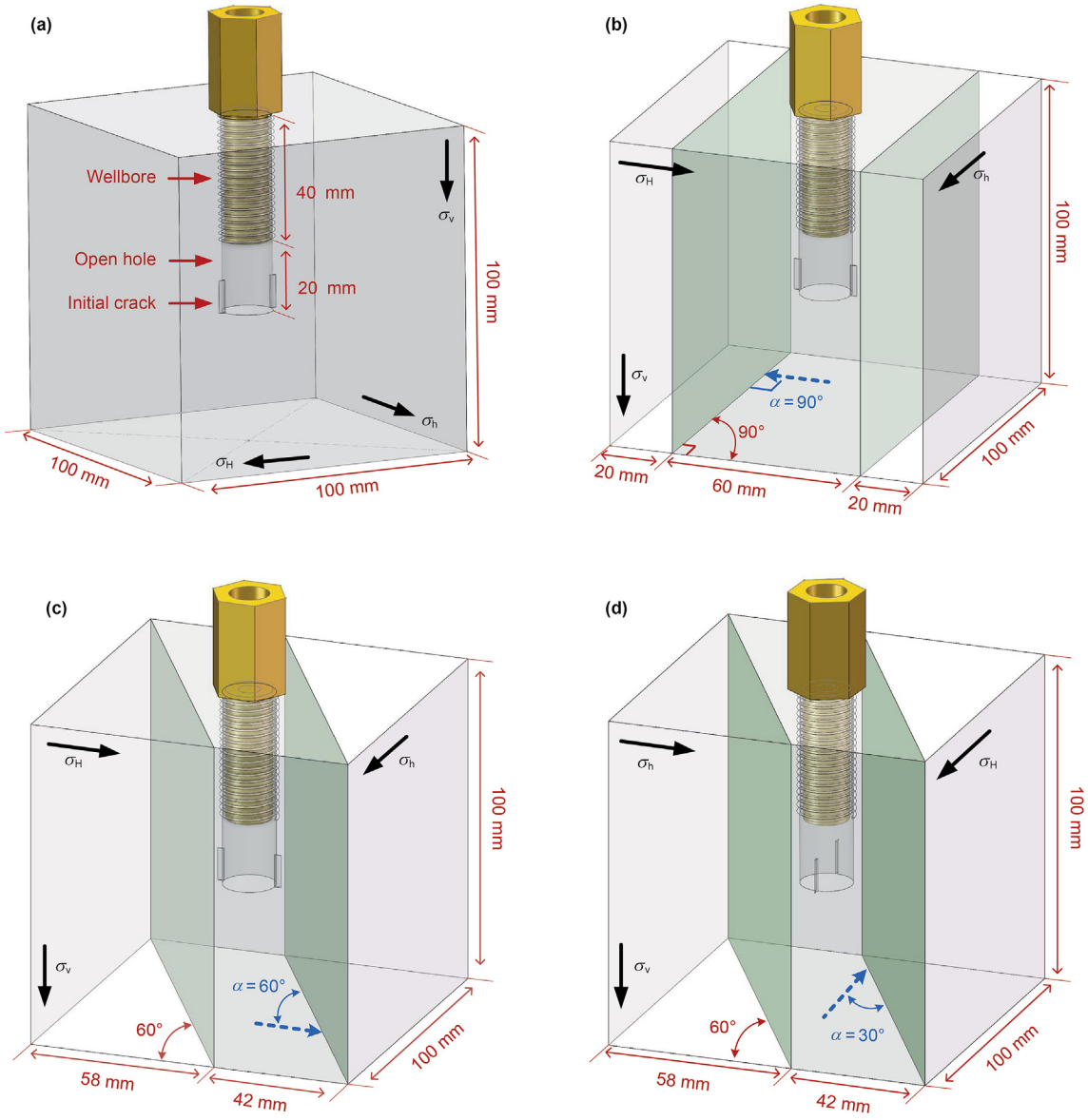

Fig. 2. Schematic of different bonding angles of PMMA specimens (**a**) Intact PMMA; (**b**) $\alpha = 30°$; (**c**) $\alpha = 60°$; (**d**) $\alpha = 90°$.

Table 1
PMMA mechanical properties.

Sample material properties	PMMA	Shale
Tensile strength, MPa	51.53	7.72
Uniaxial compressive strength, MPa	141.33	52.32
Elastic modulus, GPa	8.14	5.31
Toughness, MPa·m$^{-1/2}$	1.52	1.15
Poisson's ratio	0.41	0.29

of hydraulic fracture was stopped at the interface. Minor deflecting of hydraulic fracture was observed right after it penetrated the interface and gradually propagated parallel to the direction of maximum principal horizontal stresses. As the approaching angle down to $\theta = 30°$ (Fig. 3(c)), the hydraulic fracture was terminated at the pre-existing fracture and propagated along the interface by activating the pre-existing fracture. The finding implies that the pre-existing fracture is prone to be penetrated under high angles of approach. The test results were in great agreement with the conclusion presented by former scholars where the hydraulic fracture was prone to be arrested by natural fractures or to activate the natural fractures under a low approaching angle.

3.2. Effect of in-suit horizontal stress difference on the interaction behaviors

To investigate the effect of horizontal stress difference on fracture interaction behaviors, the injection rate ($Q = 5$ mL/min) and approaching angle ($\theta = 60°$) remain constant while the value of k_h (from 1 to 2.3) is variable. The fracture geometry of PMMA specimens was shown in Fig. 4. Three different behaviors of fracture interaction were observed in this group of tests, all the specimens generated a bi-wing hydraulic fracture from the bottom of the open hole and propagated perpendicular to the direction of minimum horizontal stress. It was noted that all the hydraulic fractures intersected the pre-existing fracture at the approximately same angle ($\theta = 60°$). When the value of k_h was equal to 2.3, the hydraulic fracture crossed both sides of pre-existing fractures and continued

Table 2
The hydraulic fracturing experimental tests scheme.

Specimen number #	Approaching angle	σ_H, MPa	σ_h, MPa	σ_v, MPa	In-situ stress difference	Injection rate, mL/min
1	90°	10	4	15	1.5	30
2	60°	10	4	15	1.5	30
3	30°	10	4	15	1.5	30
4	60°	10	5	15	1	5
5	60°	10	4	15	1.5	5
6	60°	10	3	15	2.3	5
7	60°	10	4	15	1.5	20
8	90°	10	10	0	0	5
9	90°	10	0	15	–	5

We defined α as the angle between the direction of the pre-fractured interface and the direction of maximum horizontal stress.

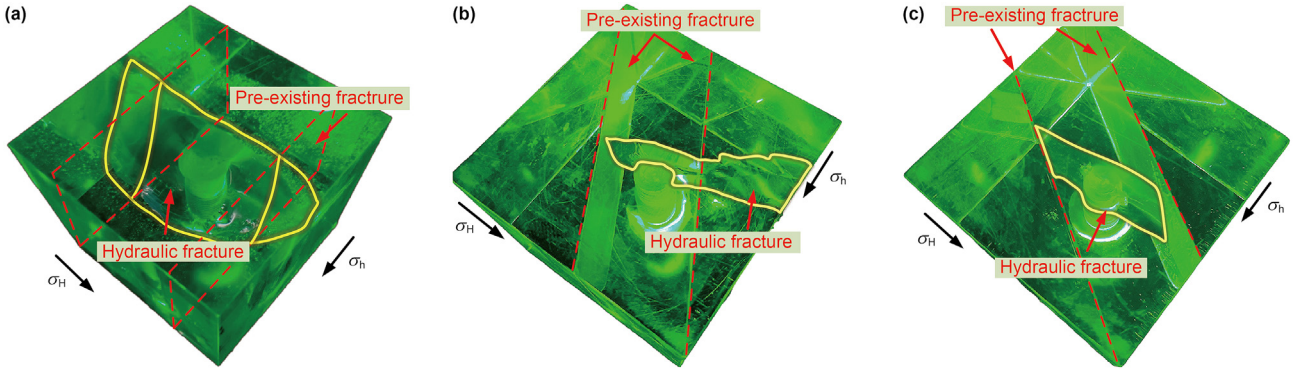

Fig. 3. The geometry of hydraulic fractures at different interaction angles (**a**) $\theta = 90°$; (**b**) $\theta = 60°$; (**c**) $\theta = 30°$.

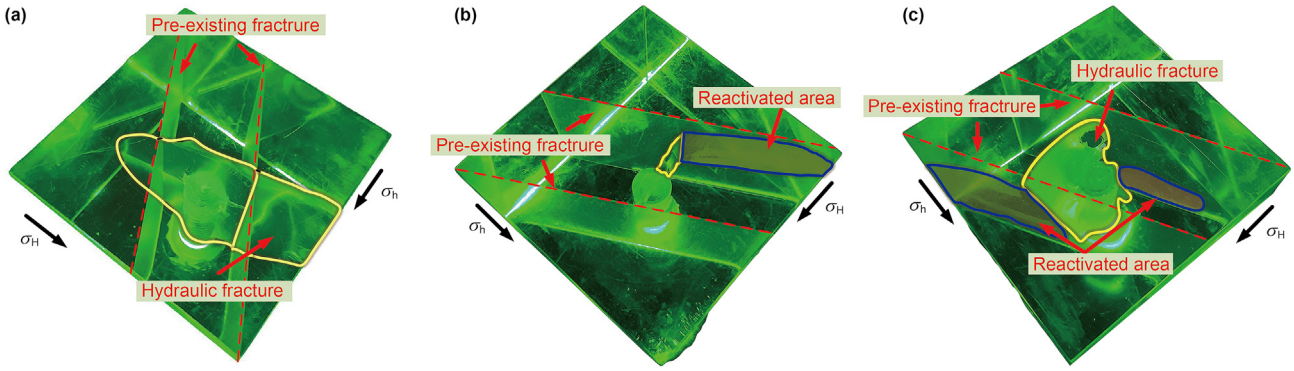

Fig. 4. Geometry of hydraulic fractures at different horizontal stress differences (**a**) $k_h = 2.3$; (**b**) $k_h = 1.5$; (**c**) $k_h = 1$.

to propagate along the direction of σ_H as was expected, and none of the pre-existing fractures was reactivated by hydraulic fracture, as shown in Fig. 4(a). With the value of k_h decreased to 1.5, only one wing hydraulic fracture was formed and impeded at the pre-existing fracture, then the hydraulic fracture propagated along the pre-existing fracture by opening the interface. For k_h equals 1, the bi-wing hydraulic fracture was initiated from the notch and extended to the pre-existing fracture parallel to the direction of the maximum horizontal stress. As the hydraulic fracture terminated at the pre-existing fracture, it started to open and dilate both sides of the pre-existing fracture and grew along the interface until one of the fracture tips reached the surface of the specimen. The blue line represented the area where the pre-existing fracture was reactivated. The test results revealed that the interaction behavior between hydraulic fracture and the pre-existing fracture was impacted by the ratio of horizontal stress difference. Under a greater value of k_h, the hydraulic fracture tends to penetrate over the interface. In contrast, the hydraulic fracture is more likely to be arrested by natural fracture under a lower value of k_h. Moreover, we observed that both sides of the natural fractures were reactivated when the k_h was equal to 1, and as the k_h increased to 1.5 only one side of the natural fractures was dilated presenting a smaller reactivated area than sample 4#. Post-test observation of sample 6# shows that only direct crossing behavior was presented without activating any of the natural fractures. The reason might be attributed to the smaller horizontal stress difference would induce higher pressure water propagating inside the samples, which promotes activating the natural fractures.

3.3. Effect of injection rate on fracture propagation

The injection rate is an important controllable factor in the reservoir stimulations, while the confining stress and rock mechanical properties are uncontrollable variables. Adjusting the

injection rate of the fracturing fluid is the primary method to optimize the effect of fracturing. A group of tests was conducted to investigate the effect of pumping rate on the interaction behaviors between hydraulic fracture and pre-existing fracture. In this group of tests, the ratio of horizontal stress difference and approaching angle are fixed to the value of 1.5 and 60°, respectively. Injection rates were set with the value of 5, 20, and 30 mL/min, respectively. It is clear from the test results that with the increase in the pumping rate, the hydraulic fracture has the inclination to cross the pre-existing fracture, as shown in Fig. 5. This is because the injection rate has a positive correlation with the fracture aperture and the stress intensity factor. With the increase of injection rate, the stress intensity factor increases accordingly. As the stress intensity factor exceeds the fracture toughness of the rock, a new fracture is expected to form at the interface. Thus, the hydraulic fracture tended to penetrate over the interface under a higher injection rate. An important fact to emphasize is that only one side of the pre-existing fracture was dilated with the flow rate of 5 mL/min and both sides of the pre-existing fractures were reactivated when the injection rate increased to 20 mL/min. Whereas, the hydraulic fracture directly crossed the interface without opening or dilating the pre-existing fracture under the injection rate of 30 mL/min. A higher flow rate might assist in reactivating the natural fractures but the reactivated area tends to reduce when the flow rate is high enough to cross over the pre-existing interface.

3.4. The process of hydraulic fracture dynamic propagation

To visualize the interaction characteristics of arresting and crossing, the high-speed camera was applied during the last two tests to record the hydraulic fracture initiation and propagation process. Fig. 6 shows the progression of the hydraulic fracture growth at different time. For sample 8#, the upper confining plate was removed, so that the fracture growth was able to be captured from the top view of the specimens, meaning that no vertical stress (σ_z) would be applied during the fracturing tests. As shown in Fig. 6(a), the hydraulic fracture was initiated from the bottom hole forming a transverse fracture (perpendicular to the wellbore) as we expected. This is because no vertical stress was applied, so hydraulic fracture would propagate along the least resistance direction (horizontal plane). It is obvious that the hydraulic fracture was impeded by the interface as it first reached the pre-existing fracture. Since the PMMA sample was not subject to vertical stress resulting the fluid pressure in the hydraulic fracture being lower than the normal stress acting on the interface, hence, the hydraulic fracture is unable to penetrate through the interface and tends to be arrested. As presented in Fig. 6(b) and (c), with the fracturing fluid continuing to pump in, the hydraulic fracture only extended laterally within the area of two interfaces until it reached the boundary of the specimen.

The strong brittleness of the PMMA leads to the propagation speed rather fast, a vacuum zone behind a leading edge of the fracture was clearly captured by the high-speed camera, as shown in Fig. 6(b), the yellow line represents the tip of the fracture and the dark dash line represents the fluid front tip. This phenomenon might cause a strong pressure gradient along the fracture meaning that high fluid pressure unable to reach the tip of a propagating hydraulic fracture. As a consequence, the hydraulic fracture is preferentially arrested rather than activating the pre-existing natural fractures.

It is unlikely to form a vertical hydraulic fracture under the strike-slip faulting stress regime ($\sigma_H > \sigma_v > \sigma_h$). In such cases, the direction of hydraulic fracture growth was not controlled by horizontal stress difference indicating that the pre-existing fracture could not be easily crossed by the hydraulic fracture. To improve the understanding of fracture crossing behaviors, we removed one of the side confining plates for recording by the high-speed camera. It was worth mentioning that the minimum horizontal stress was zero due to the lack of placing one of the side plates (sample 9#). Moreover, the vertical stress and maximum horizontal stress were set to 15 and 10 MPa, respectively. The fracture patterns were shown in Fig. 7, it is clear that as the right-wing of the fracture first arrived at the interface, it showed a strong tendency to be stopped at the interface and started to extend vertically forming a bi-wing fracture. Different from sample 8#, the right-wing of the hydraulic fracture was reinitiated at the intersection point penetrating over the pre-existing interface after the hydraulic fracture vertically grow to some extent as seen in Fig. 7(c). This is because as the hydraulic fracture started to extend vertically, the net pressure increases accordingly and eventually exceeds the pressure necessary to initiate a fracture at the intersection point. However, the left-wing of the hydraulic fracture was impeded by the bounded interface and only extended vertically. One of the possible reasons is that since one wing of the fracture has already crossed the interface, it needed less energy to extend along this direction rather than penetrating over another pre-existing interface.

We could observe from Figs. 6 and 7 that as the hydraulic fracture reached the interface, it showed a tendency to stop propagating along the original direction and started to grow laterally or vertically. The possible reason for this phenomenon could be the fully glued interface presents rather high mechanical strength impeding the hydraulic fracture penetrated through it.

3.5. Injection pressure evolution

The pressure curve can be used to evaluate the interaction

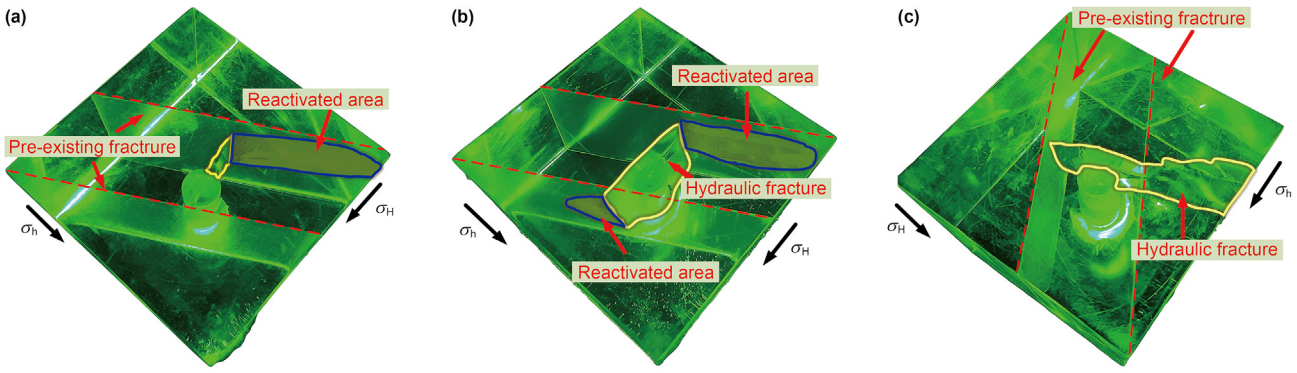

Fig. 5. Geometry of hydraulic fractures under different injection rates (**a**) Q = 5 mL/min; (**b**) Q = 20 mL/min; (**c**) Q = 30 mL/min.

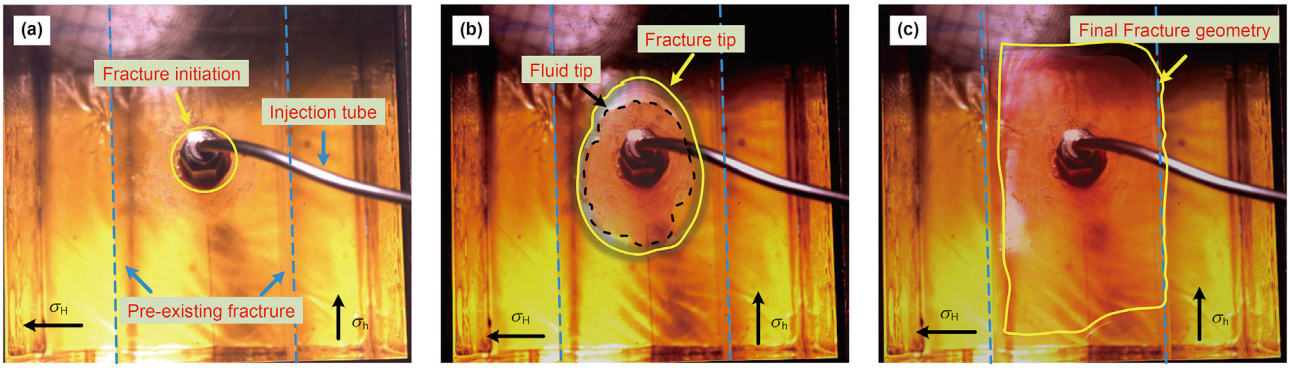

Fig. 6. The process of hydraulic fracture being arrested by pre-existing fracture at different times (**a**) 0 s; (**b**) 0.034 s; (**c**) 0.084 s.

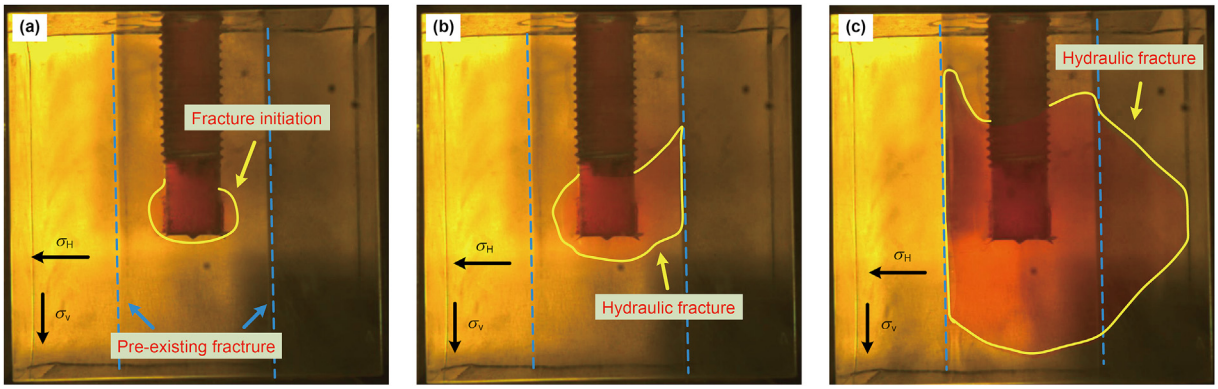

Fig. 7. The process of hydraulic fracture crossing the pre-existing fractures at different time (**a**) 0 s; (**b**) 0.031 s; (**c**) 0.078 s.

behaviors and morphology of the fracture network (Dehghan, 2020). Typically, when hydraulic fractures reach the natural fractures, the injection pressure exhibits different behaviors such as the pressure could decrease or increase with some fluctuations. Even though PMMA shows similar mechanical properties as shale, no such behaviors appeared in the pressure curve of PMMA samples, as shown in Fig. 8. It can be found that all the curves could be divided into four stages: a moderate increase, a sharp increase, a sudden drop, and a stable zone. The sharp decrease of the pressure curve indicated that PMMA samples exhibit a highly brittle behavior due to their impermeable and mechanical properties. Besides, according to the images captured by the high-speed camera in the previous section, the propagation speed of hydraulic fractures was extremely rapid due to the strong brittleness of the specimens and the scale of the test samples. That may explain why there are no obvious changes on the pressure curve when hydraulic fractures intersected with the pre-existing fracture.

In the hydraulic fracturing tests, the breakdown pressure is used to evaluate the level of fracturing difficulty. According to Fig. 8(b), the lower value of k_h, the higher the breakdown pressure. This is because as the k_h decreases, the confining stress increases accordingly, requiring higher fluid pressure to break down the rock and generate fractures. Besides, it can be seen from Fig. 8(c) that with the decrease of the injection rate, the breakdown pressure increases from 12.68 to 15.42 MPa, indicating that the injection rate has a negative correlation with the breakdown pressure of PMMA

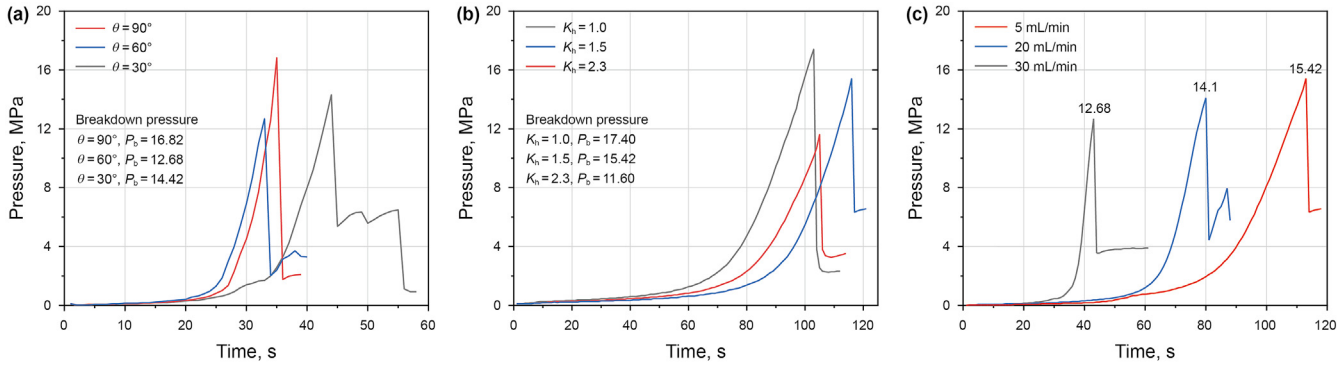

Fig. 8. Injection pressure versus time. (**a**) Injection curves at different approaching angles; (**b**) Injection curves at different horizontal stress differences; (**c**) Injection curves at different injection rates.

specimens. However, the results of the tests were not consistent with that of the natural rock (shale, sandstone) subject to hydraulic fracturing, where injection pressure exhibits a positive correlation with the pumping rate. The possible reason could be more fracturing fluid leaking off to the porous medium around the open hole, decreasing the breakdown pressure for the natural rock. Whereas, it is nearly impermeable for PMMA material.

4. Numerical simulation of hydraulic fracture interacting with pre-existing fracture

4.1. Basic theory

The cohesive zone method was first introduced in 1959, which is capable of simulating the initiation and propagation of hydraulic fractures by defining the mechanical strength of the fracture and the rock (Barenblatt, 1962; Li et al., 2017; Baykin and Golovin, 2018). The process of fracture growth, fluid flow, rock deformation, and fluid leak-off were fully coupled through the cohesive elements, and some researchers have successfully applied this method to investigate the interaction behaviors between hydraulic fracture and natural fracture. The law of material damage to the cohesive element followed the bilinear model where two damage stages were defined as shown in Fig. 9. The cohesive element presents reversible linear elastic until it reaches the material's maximum strength. Once the traction exceeds the strength limit, the strength of the cohesive element decreases linearly until the damage occurs.

The fracturing fluid within cohesive elements was assumed to be incompressible Newtonian fluid, and it was divided into the tangential flow which indicated the propagation of the fracture, and the normal flow representing the fluid leak-off into the nearby material, as indicated in Fig. 10.

The tangential flow within the fracture is governed by Eq. (2):

$$q = \frac{t^3}{12\mu}\nabla\rho \tag{2}$$

where q [m^3] is the fluid flux velocity vector, μ [Pa·s] is the viscosity of the fracturing fluid, $\nabla\rho$ [Pa] is the pore pressure gradient, and t [m] is the opening of the fracture. The normal flow is presented as

$$\begin{cases} q_t = C_t(P_i - P_t) \\ q_b = C_b(P_i - P_b) \end{cases} \tag{3}$$

where q_t [m/s] and q_b [m/s] represent the fluid flux velocity infiltrating the top and bottom cohesive elements, C_t and C_b are the top and bottom leak-off coefficients of the cohesive element surfaces, P_t [Pa] and P_b [Pa] are pore pressure of the top and bottom surface of the cohesive elements, and P_i represents the pore pressure inside the cohesive elements.

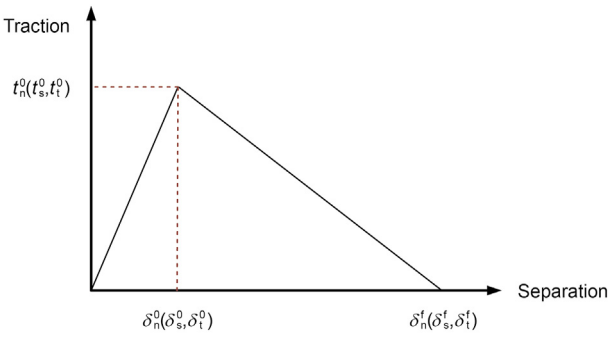

Fig. 9. Quadratic nominal stress traction-separation law (Abaqus, 2011).

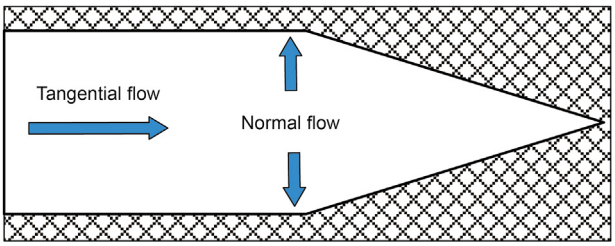

Fig. 10. Schematic diagram of fluid flow within the cohesive element (Abaqus, 2011).

4.2. Model implementation

In this work, a hydro-mechanical model was implemented by Abaqus, the hydraulic fracture and pre-existing fractures were represented by zero-thickness cohesive elements so that the fractures could initiate and propagate along the predefined path, which was represented by the yellow line in Fig. 11. To simplify the computing process and decrease simulation time, only one hydraulic fracture and a single natural fracture were embedded in the model. The injection point was placed at the beginning of the hydraulic fracture and the fracturing fluid was pumped at a constant injection rate. The approaching angles between hydraulic fracture and natural fracture were set at 30°, 60°, and 90°, which were lined up with experimental tests. According to the size of PMMA specimens, the numerical model was defined as 50 mm × 50 mm to better verify the results of hydraulic fracturing experimental tests. The model was discretized into a number of 15100 elements (CPE4P) and the intersection node of the cohesive element was able to transfer the fluid pressure from the hydraulic fracture to the natural fracture so that the hydraulic fracture would either propagate across the natural fracture or deflect into the natural fracture. The schematic models of the discretized domain are shown in Fig. 11.

4.3. Input data

In our model, the natural fractures were considered as cemented natural fractures presenting a lower value of tensile and shear strength. Compare to the frictional natural fractures, shear slippage of cemented natural fractures is not likely to occur, as a result, the shear stress of natural fractures is higher than that of the tensile stress (Zhang et al., 2020b). Based on our previous mechanical tests of the shale samples containing cemented natural fractures, the mechanical strength of rock mass is roughly two times higher than that of the cemented natural fracture. The other input parameters are in accordance with the properties of the PMMA and the data from the numerical simulations presented by other scholars (Guo et al., 2017; Li et al., 2019; Wang, 2019; Sun et al., 2022), the input data are summarized in Table 3.

4.4. Simulation results and analysis

Three models with different approaching angles (30°, 60°, 90°) were introduced to investigate the effect of the approaching angle between the natural fracture and hydraulic fracture. To be noted that the confining stress in the simulation models was aligned with the in-situ stress set by the experimental tests to verify the results of the hydraulic fracturing laboratory tests. For better visualization, the degree of element deformation was zoomed out 50 times larger than its actual damage. A summary of numerical simulation parameters was shown in Table 4. The simulation results were shown in Figs. 12–14.

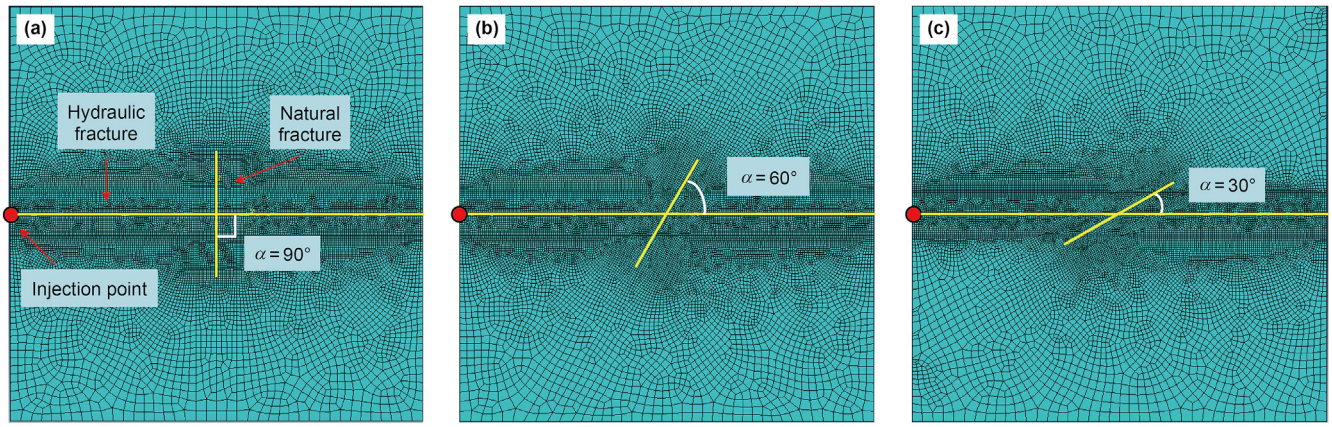

Fig. 11. Schematic model of the hydraulic fracture approaching the natural fracture at different angles (**a**) $\alpha = 90°$; (**b**) $\alpha = 60°$; (**c**) $\alpha = 30°$.

Table 3
Mechanical and hydraulic properties of the numerical model.

Categories	Variables	Values
Rock matrix	Young's modulus, GPa	8
	Poisson's ratio	0.4
	Hydraulic conductivity, $m \cdot s^{-1}$	1×10^{-13}
	Porosity	0.05
	Tensile stress, MPa	50
	Shear stress, MPa	80
Natural fracture	Tensile stress, MPa	25
	Shear stress, MPa	40
Fracturing fluid	Fluid viscosity, Pa·s	1×10^{-3}
	Specific weight, $kN \cdot m^{-3}$	9.8

Fig. 12 presented the fracture geometry under different approaching angles (30°, 60°, 90°). The results revealed that the approaching angle determines the interaction behaviors between the hydraulic fracture and natural fracture. The hydraulic fracture was stopped and arrested by the natural fracture within the approaching angle between 30° and 60°. As the fracturing fluid continued to pump in, the hydraulic fracture diverted into the pre-existing fracture as shown in Fig. 12(a) and (b). When the α increases to 90°, the natural fracture was crossed under the same confining stress. The results demonstrated that the larger the approaching angle, the easier the hydraulic fracture is to propagate through the natural fracture.

In order to study the influence of horizontal in-situ stress difference on the interaction behaviors, the injection rate and approaching angle were fixed at 5 mL/min and 60° respectively. As shown in Fig. 13, the hydraulic fracture was initiated at the injection point and propagated perpendicular to the direction of minimum horizontal stress. The natural fracture tended to impede the growth of hydraulic fracture when the horizontal stress difference is less than 1, which agrees well with the experimental results.

In the cases where larger horizontal stress differences and approaching angles are simulated, higher normal stress could be applied to the natural fracture. Therefore, large tensile stress or shear stress is required to overcome the bonding force and open up the natural fracture, resulting in the crossing behavior being more likely to occur as shown in Fig. 13(b) and (c).

Fig. 14 showed the simulation results under different injection rates, and it demonstrated that the injection rate is also an important factor in affecting the pattern of fracture networks. In this group of simulations, the in-situ stress difference and the approaching angle are fixed at the value of 1.5 and 60°, respectively. As expected, the hydraulic fracture is prone to cross the natural fractures at a higher injection rate. As shown in Fig. 14(a), under the injection rate of 30 mL/min, the hydraulic fracture crossed the natural fracture and propagated orthogonal to the direction of minimum horizontal stress. As the injection rate decreased to 5 mL/min, the hydraulic fracture tended to turn into the natural fracture, deviating from the preferential propagation direction (Fig. 14(c)).

In general, the 2D cohesive model was able to simulate hydraulic fracturing based on the finite method, and the simulation results showed a great agreement with that of the hydraulic fracturing experimental tests, which were concluded in Table 4.

5. Discussions

Ture tri-axial hydraulic fracturing experimental tests and numerical simulations were carried out to investigate the interaction behavior between pre-existing fracture and hydraulic fracture. The experimental outcomes are consistent well with the numerical results simulated by the cohesive zone method. According to the results, three different interaction modes were observed: hydraulic fracture crossed natural fracture; hydraulic fracture was arrested by activating the interface; hydraulic fracture was arrested without activating the interface.

Based on the previous study of hydraulic fracturing on natural rocks, the hydraulic fracture could cross and dilate the natural

Table 4
Experimental and numerical simulation results.

Simulation case #	Approaching angle	In-situ stress difference	Injection rate, mL/min	Simulation results	Experimental results
1	90°	1.5	30	Crossed	Crossed
2	60°	1.5	30	Arrested	Arrested
3	30°	1.5	30	Arrested	Arrested
4	60°	1	5	Arrested	Arrested
5	60°	1.5	5	Arrested	Arrested
6	60°	2.3	5	Crossed	Crossed
7	60°	1.5	20	Crossed	Crossed

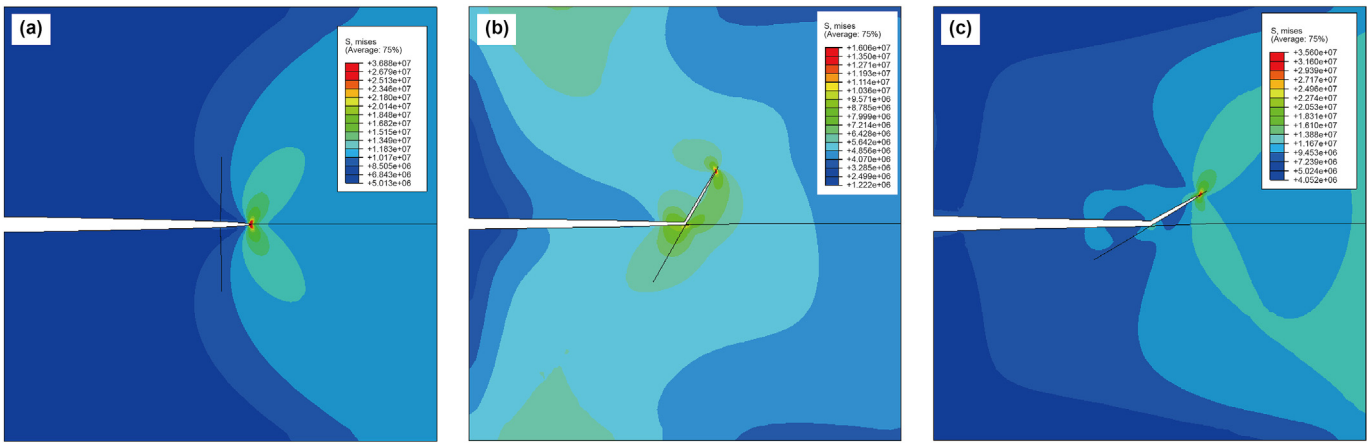

Fig. 12. The simulation results of hydraulic fracture interacting with the natural fracture at different approaching angles (**a**) $\alpha = 90°$; (**b**) $\alpha = 60°$; (**c**) $\alpha = 30°$.

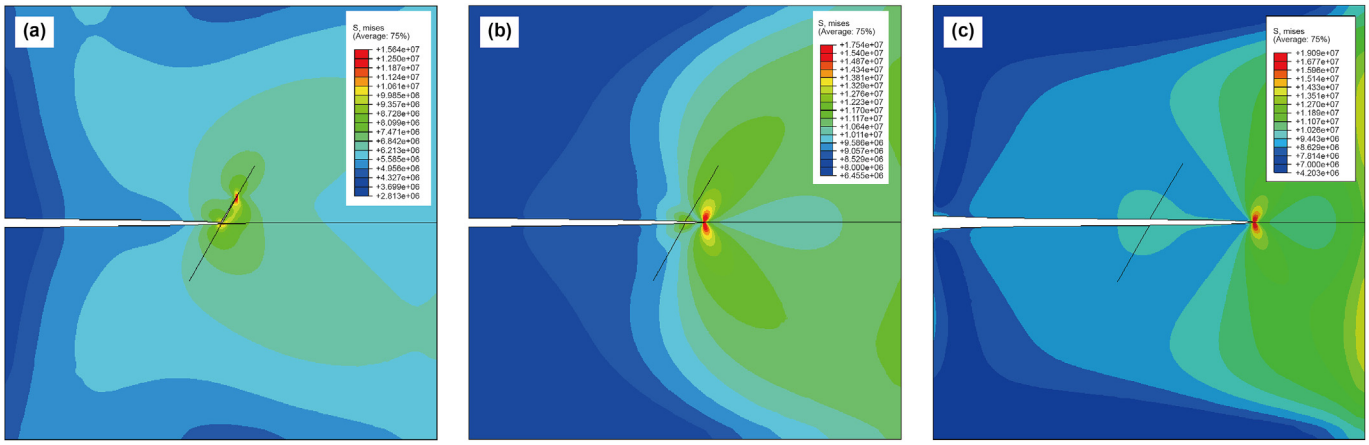

Fig. 13. The simulation results of hydraulic fracture interacting with natural fracture at different horizontal stress differences (**a**) $k_h = 1$, (**b**) $k_h = 1.5$, (**c**) $k_h = 2.3$.

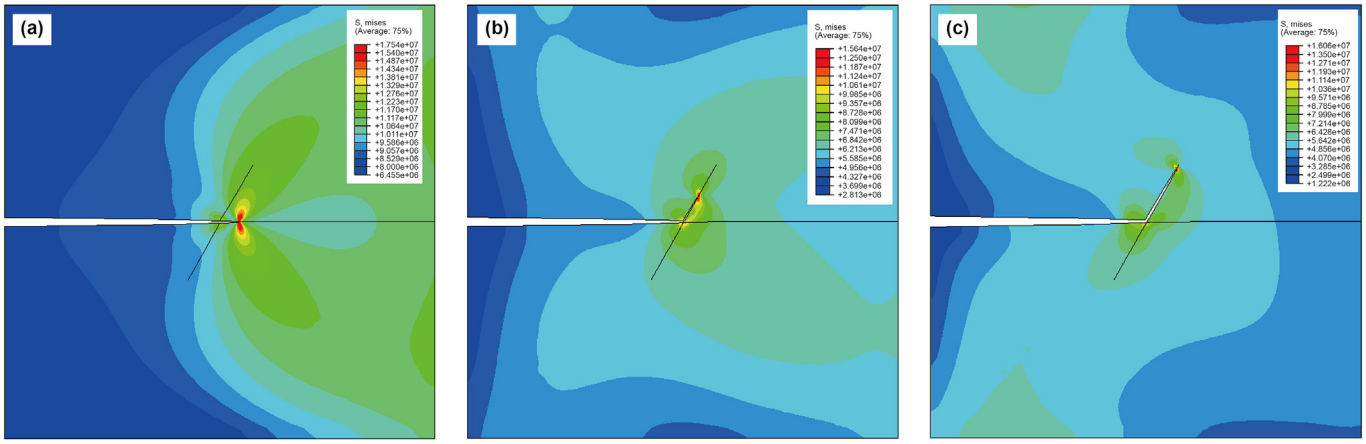

Fig. 14. The simulation results of hydraulic fracture interacting with the natural fracture at different injection rates (**a**) $Q = 30$ mL/min; (**b**) $Q = 20$ mL/min; (**c**) $Q = 5$ mL/min.

fractures simultaneously, as shown in Fig. 15(b). Whereas, such behavior did not exist in our study. Previous research showed that the properties of the natural fractures (the mechanical strength of the natural fractures, the fracture frictional properties, etc.) have a huge influence on the fracture interaction behaviors as well (Kolawole and Ispas, 2020; Tang et al., 2023). The reason for the discrepancy might be that the pre-existing interface in our tests was simulated by gluing plates together, presenting the high cemented strength with extremely low permeability within the interface, meaning that the pre-manufactured natural fractures tend not to be dilated when the fluid approach the intersection point.

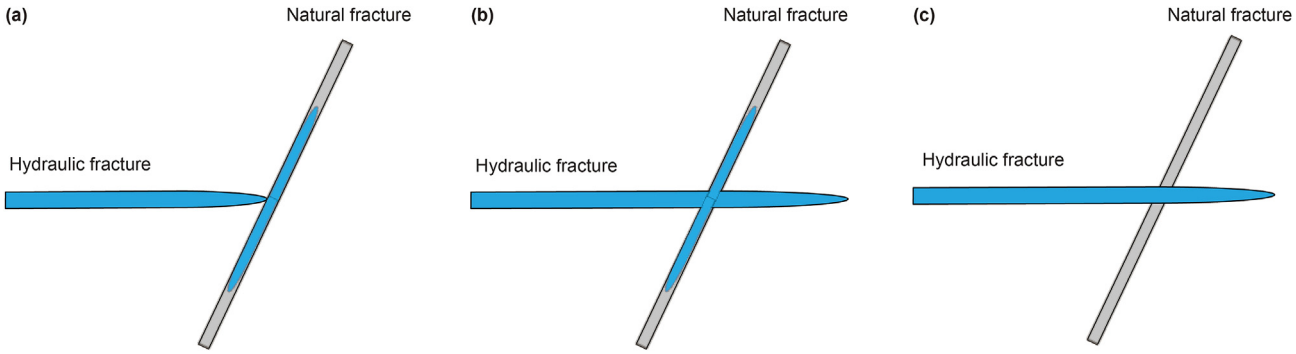

Fig. 15. Interaction mode between hydraulic fracture and natural fracture. (**a**) Arresting; (**b**) Crossing with dilation; (**c**) Crossing without dilation.

It should also be aware that as we were conducting hydraulic fracturing experimental tests, there were a few tests inconsistent with the results of the others. According to the studies, we concluded that hydraulic fractures are prone to cross the natural fracture at a higher approaching angle and horizontal stress difference, which was also confirmed by the other researchers. In the case of sample 6, the crossing behavior was observed under the approaching angle of 60°. We expected identical interaction behavior to occur as the approaching angle increased from 60° to 90° while other conditions remained the same. However, the hydraulic fracture was arrested by pre-existing fracture even under a higher approaching angle than that of sample 6, as shown in Fig. 16. One possible reason is that the distance between the wellbore and the natural fracture could influence the interaction mode. Some scholars found that with the long distance between the injection point and the natural fractures, the hydraulic fracture is more likely to be stopped and impeded. Another possible reason could be that as the hydraulic fracture reached the interface, the stress of the fracture tip is not high enough to penetrate over the interface, so it would be not able to propagate along the original direction, resulting in extension vertically until it grew to the up or bottom surface of the specimens, which was similar with the fracture propagation process in samples 8# and 9#.

Weak planes such as natural fractures and bedding planes commonly exist in shale gas formation. The hydraulic fracturing mechanism is a complex problem, especially when interacting with natural fractures. How to fracture the target zone effectively and create a complex fracture network still remains challenging. Pump displacement is one of the controllable parameters which could be modified by field engineers in field applications. It is believed that there could be a certain displacement rate that enables the hydraulic fracture to cross the natural fracture and activate it simultaneously. In other words, finding the proper injection rate of the shale gas reservoir is the key to generating a complex fracture network. Consequently, more work needs to be done to build a solid connection between the field application and the laboratory experiments.

In addition, there are still other parameters we did not take into account when hydraulic fracture interacts with the natural fracture beside the factors (horizontal stress difference, approaching angle, injection rate) we have studied. For instance, only one single pre-existing fracture was simulated in our tests, whereas, it may exist a complex natural fracture system underground due to different multi-stage tectonic movements. Moreover, it is believed that the mechanical property of the natural fracture also has a substantial effect on the behavior of the fracture interaction. There are two types of natural fractures in the shale reservoir, which are frictional natural fractures and cemented natural fractures. According to the field research of shale reservoirs, most of the closed natural fractures are not entirely separated, but with cementation strength. Therefore, in our work, the prefabricated natural fractures were fully cemented with high-strength glue at a certain thickness which would hugely influence the frictional properties of prefabricated natural fractures. However, the frictional coefficient between the cement and the PMMA interface is hardly controllable and measurable which was neglected in our work. Despite the produced natural fractures within the samples did not consider the frictional properties, it still allows us to present the interaction process between cemented natural fractures and hydraulic fractures. Nonetheless, the frictional behavior of the cemented natural fractures should be considered and needs to do further research on how to produce natural fractures with controllable and adjustable interface properties in the future.

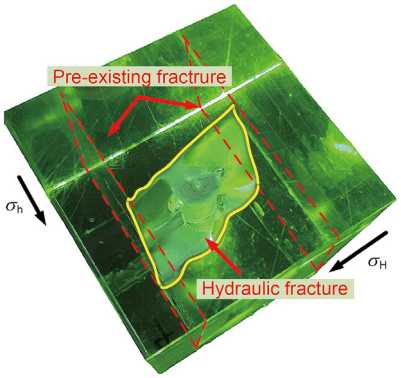

Fig. 16. Geometry of hydraulic fracture being arrested by pre-existing fracture.

6. Conclusions

In this paper, we conducted true tri-axial hydraulic fracturing laboratory tests on PMMA specimens, and a 2D fracture interaction model was developed based on the cohesive zone method to study the interaction behaviors between hydraulic fracture and natural fracture. Bonding interfaces were pre-set in the PMMA specimens to simulate the natural fractures. Direct observations from the specimens and stress contour of the simulation results give us insight into the interaction behaviors between hydraulic fracture and pre-existing fracture. The geometry of the fracture network was analyzed and the main factors influencing the fracture interaction behaviors were studied. Moreover, the real-time injection pressure and the fracture dynamic propagation process were also discussed. The conclusions are drawn as follows:

(1) The hydraulic fractures were initiated at the notch and propagated along the direction of the maximum horizontal stress. Three main interaction behaviors were obtained when the hydraulic fracture intersected with the pre-existing fracture: crossing, being arrested by reactivating the pre-existing fracture, and being arrested without dilating the pre-existing fracture.
(2) Crossing behavior is more likely to occur with the increase of approaching angle, horizontal stress difference, and injection rate.
(3) Higher flow rate might assist in reactivating the natural fractures where both sides of the pre-existing fractures were reactivated as the injection rate increased from 5 to 20 mL/min. However, the reactivated area tends to reduce when the flow rate is high enough to cross over the pre-existing interface.
(4) The evolution of hydraulic fracture recorded by high-speed camera showed that hydraulic fractures show a tendency to extend vertically rather than along the direction of maximum horizontal stress when they are first terminated at the interface.
(5) When the hydraulic fracture penetrated over the pre-existing interface, the dilation of the interface is not likely to occur due to the interface presenting high cemented strength.

Declaration of competing interest

The authors declare that they have no known competing financial interests or personal relationships that could have appeared to influence the work reported in this paper.

Acknowledgment

The authors would like to acknowledge the financial support from Major Program of the National Natural Science Foundation of China (Grant No. 52192621), the National Natural Science Foundation of China for Major International (Regional) Joint Research Project (Grant No. 52020105001), Major Science and Technology Project of Yunnan Province (Grant No. 202302AF080001) and Beijing Outstanding Young Scientist Program (Grant No. BJJWZYJH01201911414038).

References

Abaqus, 2011. User's Manual, Version 6.11. Dassault Systemes.
Barenblatt, G.I., 1962. The mathematical theory of equilibrium cracks in brittle fracture. Adv. Appl. Mech. 7 (1), 55–129. https://doi.org/10.1016/S0065-2156(08)70121-2.
Baykin, A.N., Golovin, S.V., 2018. Application of the fully coupled planar 3D poroelastic hydraulic fracturing model to the analysis of the permeability contrast impact on fracture propagation. Rock Mech. Rock Eng. 51 (10), 3205–3217. https://doi.org/10.1007/s00603-018-1575-1.
Cong, Z., Li, Y., Pan, Y., et al., 2022. Study on CO_2 foam fracturing model and fracture propagation simulation. Energy, 121778. https://doi.org/10.1016/j.energy.2021.121778.
Dehghan, A.N., 2020. An experimental investigation into the influence of pre-existing natural fracture on the behavior and length of propagating hydraulic fracture. Eng. Fract. Mech. 240. https://doi.org/10.1016/j.engfracmech.2020.107330.
Dong, H., Zhang, G., Liu, S., et al., 2018. Influence of multiple natural fractures on hydraulic fracture propagation in fractured reservoir. In: 52nd US Rock Mechanics/Geomechanics Symposium. OnePetro.
Dong, J., Yuan, G., Wang, Y., et al., 2021. Experimental study of multi-timescale crack blunting in hydraulic fracture. Petrol. Sci. 18 (1), 234–244. https://doi.org/10.1007/s12182-020-00479-1.
Fatahi, H., Hossain, M., Sarmadivaleh, M., 2017. Numerical and experimental investigation of the interaction of natural and propagated hydraulic fracture. J. Nat. Gas Sci. Eng. 37409–424. https://doi.org/10.1016/j.jngse.2016.11.054.
Frash, L.P., 2014. Laboratory-scale Study of Hydraulic Fracturing in Heterogeneous Media for Enhanced Geothermal Systems and General Well Stimulation. Colorado School of Mines.
Fu, P., Schoenball, M., Ajo, J.B., et al., 2021. Close observation of hydraulic fracturing at EGS Collab Experiment 1: fracture trajectory, microseismic interpretations, and the role of natural fractures. J. Geophys. Res. Solid Earth 126 (7), 2020–20840. https://doi.org/10.1029/2020JB020840.
Fu, W., Ames, B.C., Bunger, A.P., et al., 2015. An experimental study on interaction between hydraulic fractures and partially-cemented natural fractures. In: 49th US Rock Mechanics/Geomechanics Symposium. OnePetro.
Gale, J.F., Reed, R.M., Holder, J., 2007. Natural fractures in the Barnett Shale and their importance for hydraulic fracture treatments. AAPG Bull. 91 (4), 603–622. https://doi.org/10.1306/11010606061.
Gale, J.F.W., Laubach, S.E., Olson, J.E., et al., 2014. Natural fractures in shale: a review and new observations. AAPG Bull. 98 (11), 2165–2216. https://doi.org/10.1306/08121413151.
Groenenboom, J., Duijndam, A.J.W., Fokkema, J.T., 1995. Monitoring the width of hydraulic fractures with acoustic waves. Eaeg Meeting 63 (1), 139–148. https://doi.org/10.3997/2214-4609.201409206.
Gu, H., Weng, X., Lund, J., et al., 2012. Hydraulic fracture crossing natural fracture at nonorthogonal angles: a criterion and its validation. SPE Prod. Oper. 27 (1), 20–26. https://doi.org/10.2118/139984-PA.
Guo, J., Luo, B., Lu, C., et al., 2017. Numerical investigation of hydraulic fracture propagation in a layered reservoir using the cohesive zone method. Eng. Fract. Mech. 186195–186207. https://doi.org/10.1016/j.engfracmech.2017.10.013.
Guo, T., Zhang, S., Qu, Z., et al., 2014. Experimental study of hydraulic fracturing for shale by stimulated reservoir volume. Fuel 128373–128380. https://doi.org/10.1016/j.fuel.2014.03.029.
Hong, C., Yang, R., Huang, Z., et al., 2020. Visualization of Fracture Initiation Behavior during Liquid Nitrogen Fracturing in Geothermal Wells. World Geothermal Congress.
Hou, B., Chen, M., Cheng, W., et al., 2016. Investigation of hydraulic fracture networks in shale gas reservoirs with random fractures. Arabian J. Sci. Eng. 41 (7), 2681–2691. https://doi.org/10.1007/s13369-015-1829-0.
Kolawole, O., Ispas, I., 2020. Interaction between hydraulic fractures and natural fractures: current status and prospective directions. J. Pet. Explor. Prod. Technol. 10 (4), 1613–1634. https://doi.org/10.1007/s13202-019-00778-3.
Li, J., Dong, S., Hua, W., et al., 2019. Numerical investigation of hydraulic fracture propagation based on cohesive zone model in naturally fractured formations. Processes 7 (1), 28. https://doi.org/10.3390/pr7010028.
Li, M., Zhou, F., 2022. Multi-fracture initiation sequence and breakdown pressure in horizontal wells during TDPF: a visualization experimental investigation based on PMMA. J. Petrol. Sci. Eng. 110645. https://doi.org/10.1016/j.petrol.2022.110645.
Li, Y., Deng, J., Liu, W., et al., 2017. Modeling hydraulic fracture propagation using cohesive zone model equipped with frictional contact capability. Comput. Geotech. 9158–9170. https://doi.org/10.1016/j.compgeo.2017.07.001.
Li, Y., Long, M., Tang, J., et al., 2020. A hydraulic fracture height mathematical model considering the influence of plastic region at fracture tip. Petrol. Explor. Dev. 47 (1), 175–185. https://doi.org/10.11698/PED.2020.01.17.
Li, Z., Zang, A., 2021. Laboratory hydraulic fracturing experiments on crystalline rock for geothermal purposes. Earth Sci. Rev. 216, 103580. https://doi.org/10.1016/j.earscirev.2021.103580.
Liu, N., Zou, Y., Ma, X., et al., 2019. Study of hydraulic fracture growth behavior in heterogeneous tight sandstone formations using CT scanning and acoustic emission monitoring. Petrol. Sci. 16 (2), 396–408. https://doi.org/10.1007/s12182-018-0290-6.
Liu, Y., Tang, D., Xu, H., et al., 2022a. Effect of interlayer mechanical properties on initiation and propagation of hydraulic fracturing in laminated coal reservoirs. J. Petrol. Sci. Eng. 208, 109381. https://doi.org/10.1016/j.petrol.2021.109381.
Liu, Z., Pan, Z., Li, S., et al., 2022b. Study on the effect of cemented natural fractures on hydraulic fracture propagation in volcanic reservoirs. Energy 241, 122845. https://doi.org/10.1016/j.energy.2021.122845.
Memon, S., Feng, R., Ali, M., et al., 2022. Supercritical CO_2-Shale interaction induced natural fracture closure: implications for $scCO_2$ hydraulic fracturing in shales. Fuel 313, 122682. https://doi.org/10.1016/j.fuel.2021.122682.
Roshankhah, S., Marshall, J.P., Tengattini, A., et al., 2018. Neutron imaging: a new possibility for laboratory observation of hydraulic fractures in shale? Géotech. Lett. 8 (4), 316–323. https://doi.org/10.1680/jgele.18.00129.
Roshankhah, S., Rubino, V., Marshall, J.P., et al., 2019. Monitoring laboratory hydraulic fractures in pre-fractured shale using high-resolution optical and neutron imaging techniques. In: 53rd U.S. Rock Mechanics/Geomechanics Symposium. OnePetro.
Sun, T., Zeng, Q., Xing, H., 2022. A quantitative model to predict hydraulic fracture propagating across cemented natural fracture. J. Petrol. Sci. Eng. 208, 109595. https://doi.org/10.1016/j.petrol.2021.109595.
Tang, X., Zhu, H., Li, K., 2023. A FEM-DFN-based complex fracture staggered propagation model for hydraulic fracturing of shale gas reservoirs. Nat. Gas. Ind. 43 (1), 162–176. https://doi.org/10.3787/j.issn.1000-0976.2023.01.016.
Wang, H., 2019. Hydraulic fracture propagation in naturally fractured reservoirs: complex fracture or fracture networks. J. Nat. Gas Sci. Eng. 68, 102911. https://doi.org/10.1016/j.jngse.2019.102911.
Wang, W., Olson, J.E., Prodanović, M., et al., 2018. Interaction between cemented natural fractures and hydraulic fractures assessed by experiments and numerical simulations. J. Petrol. Sci. Eng. 167506–167516. https://doi.org/10.1016/j.petrol.2018.03.095.

Wu, R., Bunger, A.P., Jeffrey, R.G., et al., 2008. A comparison of numerical and experimental results of hydraulic fracture growth into a zone of lower confining stress. In: 53rd U.S. Rock Mechanics/Geomechanics Symposium. OnePetro.
Xie, J., Tang, J., Yong, R., et al., 2020. A 3-D hydraulic fracture propagation model applied for shale gas reservoirs with multiple bedding planes. Eng. Fract. Mech. 228, 106872. https://doi.org/10.1016/j.engfracmech.2020.106872.
Xie, Z., Huang, Z., Xiong, J., et al., 2022. The influence of natural fractures on the propagation of hydraulic fractures in hot dry rock. Nat. Gas. Ind. 4 (4), 42. doi: 10.3787/j.issn.1000-0976.2022.04.006 (in Chinese).
Xie, Z., Wu, X., Huang, Z., et al., 2021. A visualization study on interaction between hydraulic fractures and natural fractures. In: 55th U.S. Rock Mechanics/Geomechanics Symposium. OnePetro.
Zeng, Y., Zhang, X., Zhang, B., 2015. Stress redistribution in multi-stage hydraulic fracturing of horizontal wells in shales. Petrol. Sci. 12 (4), 628–635. https://doi.org/10.1007/s12182-015-0048-3.
Zhang, F., An, M., Zhang, L., et al., 2020a. Effect of mineralogy on friction-dilation relationships for simulated faults: implications for permeability evolution in caprock faults. Geosci. Front. 11 (2), 439–450. https://doi.org/10.1016/j.gsf.2019.05.014.
Zhang, J., Li, Y., Pan, Y., et al., 2021. Experiments and analysis on the influence of multiple closed cemented natural fractures on hydraulic fracture propagation in a tight sandstone reservoir. Eng. Geol. 281, 105981. https://doi.org/10.1016/j.enggeo.2020.105981.
Zhang, Q., Zhang, X., Sun, W., 2020b. A review of laboratory studies and theoretical analysis for the interaction mode between induced hydraulic fractures and pre-existing fractures. J. Nat. Gas Sci. Eng. 86 (B6), 103719. https://doi.org/10.1016/j.jngse.2020.103719.
Zhang, S., Lei, X., Zhou, Y., et al., 2015. Numerical simulation of hydraulic fracture propagation in tight oil reservoirs by volumetric fracturing. Petrol. Sci. 12 (4), 674–682. https://doi.org/10.1007/s12182-015-0055-4.
Zhao, P., Xie, L., Fan, Z., et al., 2021. Mutual interference of layer plane and natural fracture in the failure behavior of shale and the mechanism investigation. Petrol. Sci. 18 (2), 618–640. https://doi.org/10.1007/s12182-020-00510-5.
Zhao, P., Xie, L., Ge, Q., et al., 2020a. Numerical study of the effect of natural fractures on shale hydraulic fracturing based on the continuum approach. J. Petrol. Sci. Eng. 189, 107038. https://doi.org/10.1016/j.petrol.2020.107038.
Zhao, X., Zhou, L., Pu, X., et al., 2020b. Formation conditions and enrichment model of retained petroleum in lacustrine shale: a case study of the Paleogene in Huanghua depression, Bohai Bay Basin, China. Petrol. Explor. Dev. 47 (5), 916–930. https://doi.org/10.1016/S1876-3804(20)60106-9.
Zhou, D., Zhang, G., Zhao, P., et al., 2018. Effects of post-instability induced by supercritical CO2 phase change on fracture dynamic propagation. J. Petrol. Sci. Eng. 166, 358–366. https://doi.org/10.1016/j.petrol.2017.12.066.
Zhou, J., Chen, M., Jin, Y., et al., 2007. Experimental study on propagation mechanism of hydraulic fracture in naturally fractured reservoir. Acta Pet. Sin. 28 (5), 109. https://doi.org/10.1016/S1872-5813(07)60034-6.
Zhou, J., Jin, Y., Chen, M., 2010. Experimental investigation of hydraulic fracturing in random naturally fractured blocks. Int J Rock Mech Min 47 (7), 1193–1199. https://doi.org/10.1016/j.ijrmms.2010.07.005.
Zhou, T., Zhang, S., Feng, Y., et al., 2016. Experimental study of permeability characteristics for the cemented natural fractures of the shale gas formation. J. Nat. Gas Sci. Eng. 29, 345–354. https://doi.org/10.1016/j.jngse.2016.01.005.
Zou, Y., Zhang, S., Ma, X., et al., 2016a. Numerical investigation of hydraulic fracture network propagation in naturally fractured shale formations. J. Struct. Geol. 84, 1–13. https://doi.org/10.1016/j.jsg.2016.01.004.
Zou, Y., Zhang, S., Zhou, T., et al., 2016b. Experimental investigation into hydraulic fracture network propagation in gas shales using CT scanning technology. Rock Mech. Rock Eng. 49 (1), 33–45. https://doi.org/10.1007/s00603-015-0720-3.